CMLS, Cell. Mol. Life Sci. 62 (2005) 446–460
1420-682X/05/040446-15
DOI 10.1007/s00018-004-4422-3
© Birkhäuser Verlag, Basel, 2005

CMLS Cellular and Molecular Life Sciences

## Research Article

# Binding site of activators of the cystic fibrosis transmembrane conductance regulator in the nucleotide binding domains

**O. Moran[a,] *, L. J. V. Galietta[b] and O. Zegarra-Moran[b]**

[a] Istituto di Biofisica, CNR, Via DeMarini 6, 16149 Genova (Italy), Fax: + 39 0106475500,
e-mail: moran@ge.ibf.cnr.it
[b] Laboratorio di Genetica Molecolare, Istituto G. Gaslini, L.go Gerolamo Gaslini 5, 16148 Genova (Italy)

Received 21 September 2004; received after revision 6 December 2004; accepted 10 December 2004

**Abstract.** The use of substances that could activate the defective chloride channels of the mutant cystic fibrosis transmembrane conductance regulator (CFTR) has been suggested as possible therapy for cystic fibrosis. Using epithelia formed by cells stably transfected with wild-type or mutant (G551D, G1349D) CFTR, we estimated the apparent dissociation constant, $K_D$, of a series of CFTR activators by measuring the increase in the apical membrane current. Modification of apparent $K_D$ of CFTR activators by mutations of the nucleotide-binding domains (NBDs) suggests that the binding site might be in these regions. The human NBD structure was predicted by homology with murine NBD1. An NBD1-NBD2 complex was constructed by overlying monomers to a bacterial ABC transporter NBD dimer in the 'head-to-tail' conformation. Binding sites for CFTR activators were predicted by molecular docking. Comparison of theoretical binding free energy estimated in the model to free energy estimated from the apparent dissociation constants, $K_D$, resulted in a remarkably good correlation coefficient for one of the putative binding sites, located in the interface between NBD1 and NBD2.

**Key words.** ABC transporters; cystic fibrosis; molecular docking; molecular modeling; chloride channel.

The cystic fibrosis transmembrane conductance regulator (CFTR) is a single-polypeptide product of a gene defective in cystic fibrosis (CF), a life-threatening disease [1]. CFTR belongs to the family of ATP-binding cassette (ABC) transporters. All known ABC transporters seem to require two, well-conserved, nucleotide-binding domains (NBDs) and at least two less conserved transmembrane domains (TMDs) to function normally [2, 3]. In the case of CFTR, a single gene encodes all domains. Accordingly, $NH_2$- and COOH-terminal halves of CFTR both contain a TMD followed by an NBD, and both parts are linked by a cytoplasmic regulatory domain [for a review see refs 4, 5]. CFTR, which has a key physiological role in the apical membrane of various epithelia, forms a $Cl^-$ channel activated by ATP following phosphorylation by cAMP-dependent protein kinase.

Various CF-correlated mutations of CFTR produce an impairment of the gating mechanisms of the chloride channel (type III mutations; see www.genet.sickkids.on.ca/cftr/). They result in a strongly decreased epithelial chloride secretion due to a reduction in the open-channel probability. A pharmacological increase of CFTR-$Cl^-$ current by small organic molecules, called CFTR activators, has been proposed as a therapeutic strategy [6]. Numerous CFTR activators, belonging to different chemical families, have been identified [7–13]. Several reports have concluded that different CFTR activators work with the same mechanism, probably binding at the NBDs [12, 14–16]. Interestingly, many of the most severe mutations that cause CF occur within the NBDs [17], and

* Corresponding author.

significant changes in the affinity of CFTR openers have been observed when tested in cellular preparations expressing CF-related mutations in the NBDs of CFTR [18, 19].

The design of more adequate potentially therapeutic drugs will be strongly facilitated by the availability of a molecular model of the target protein. In the absence of a three-dimensional structure of human CFTR, we have attempted to construct a molecular model of each of the NBDs of CFTR, based on the crystallized structure of murine NBD1 [20]. The NBDs exhibit regions with a high degree of sequence similarity across the ABC family, implying a conserved structure and function [21]. According to the X-ray diffraction data from bacterial NBD crystals, the functional conformation of the NBDs would imply a close interaction between the two NBDs, in the 'head-to-tail' conformation [3, 22–27]. Electrophysiological [23] and biochemical [28–30] studies of wild-type (WT) and single point mutants of NBDs of CFTR support the idea that NBD1 and NBD2 interact closely in a dimer-like conformation, similar to observations on other ABC proteins [22, 26, 27, 31, 32]. Hence, we have modeled the human NBD dimer by arranging the two monomers in positions equivalent to those of the MJ0796 NBD dimer [26, 27], an ABC transporter from *Methanococus jannaschi.*

Binding sites for several CFTR activators to the model were predicted by docking techniques, and empirical binding free energy differences ($\Delta G_{model}$) estimated from models were compared to experimental free energy differences ($\Delta G_{exp}$) estimated from the apparent dissociation curves obtained from apical membrane current. The good correlation between the theoretical and experimental data strongly suggests that CFTR activators bind to a position in the NBD-NBD interface. This model may be used to predict the affinity of novel CFTR activators in silico.

## Materials and methods

### Cell cultures

Fisher rat thyroid (FRT) cells expressing WT, G551D or G1349D CFTR were cultured on 60-mm petri dishes with Coon's modified F12 containing 5% fetal bovine serum, 2 mM L-glutamine, 50 U/ml penicillin, 50 µg/ml streptomycin and 600 µg/ml zeocin, as previously described [18]. For Ussing chamber experiments, cells were seeded at high density ($5\times10^5$ cells/cm$^2$) on Snapwell inserts (Costar; Corning) and maintained at 37 °C in a 5% $CO_2$/95% air atmosphere. Apical and basolateral media were replaced every 48 h. Transepithelial resistance was measured daily with an epithelial voltohmmeter (Millipore-ERS; Millipore) using chopstick-like electrodes. After 4–7 days, FRT monolayers developed a transepithelial resistance in the range of 2–4 kΩ cm$^2$. Experiments were done at days 6–8 after seeding.

### Electrophysiology

Filters were mounted into a Ussing-like vertical diffusion chamber (Corning; Costar). The apical chamber was bathed with a low-$Cl^-$-containing solution (in mM): 65 NaCl, 65 Na gluconate, 1.5 $KH_2PO_4$, 2.7 KCl, 0.5 $MgCl_2$, 2 $CaCl_2$, 10 HEPES-Na and 10 glucose (pH 7.4). The basolateral chamber was instead bathed with (in mM): 130 NaCl, 1.5 $KH_2PO_4$, 2.7 KCl, 0.5 $MgCl_2$, 1 $CaCl_2$, 10 HEPES-Na and 10 glucose (pH 7.4). The basolateral membrane of FRT epithelia was permeabilized with 250 µg/ml amphotericin B and a transepithelial $Cl^-$ gradient was applied as previously reported [18, 33]. Membrane permeabilization was monitored measuring the current response to a 10-mV stimulus. The resistance progressively decreased and reached a stable value after 30–40 min. We assume this is the condition for maximal permeabilization. Experiments were done at 37 °C and solutions were bubbled with air. The transepithelial potential difference (PD) was short-circuited at 0 mV with a voltage-clamp amplifier (DVC-1000; World Precision Instruments) connected to the chambers through Ag-AgCl electrodes and agar bridges. CFTR activators were added only to the apical side, and the short-circuit current (Isc) measured. If not otherwise specified, currents were always measured in the presence of 20 µM 8-(4-chlorophenylthio)-adenosine 3′5′-cyclic monophosphate (CPTcAMP).

### Analysis of the effects of CFTR activators

We considered the effect of a given compound as the current increase over the current elicited by CPTcAMP, Isc(0). Hence, for each CFTR activator concentration, current due to CPTcAMP was subtracted, and the dose-response curves were fitted with:

$$\mathrm{Isc} - \mathrm{Isc}(0) = I_{max}\left(\frac{1}{1+(K_D/[C])^n}\right)\left(1-\frac{1}{1+(K_i/[C])}\right)$$

where $I_{max}$ is the maximum stimulated current, [C] is the CFTR activator concentration, $K_D$ is the concentration that gives half of the maximal effect or the 'apparent dissociation constant' for CFTR activation, n is the cooperativity coefficient and $K_i$ is the apparent dissociation constant for the inhibitory effect. As for many substances, besides activation, an apparent inhibition was also observed, dose-response curves were fitted according to a three-state hypothesis, assuming that two different sites are occupied to activate and inhibit the Isc current [34]. Data were fitted using the Levenberg-Marquardt algorithm, a form of non-linear, least-squares fitting, as implemented in IgorPro (Wavemetrics).

### Molecular modeling

Molecular models for the WT or mutant NBDs of human CFTR were done by homology to the mouse NBD1 [20] using Modeller [35]. The dimeric conformation of the

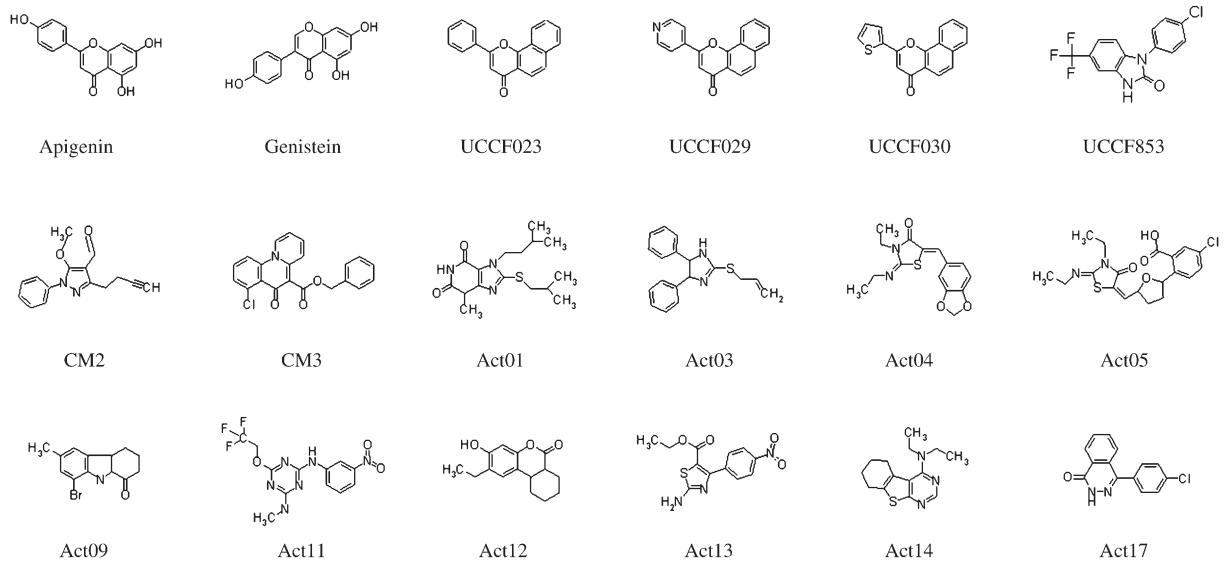


Figure 1. Chemical structure of the CFTR activators analyzed.

two NBDs was obtained fitting the NBD monomers on the dimeric structure of the putative ABC transporter MJ0796 cloned from an archeobacterium [26, 27], using the McLachlan algorithm [36] as implemented in the program ProFit (www.bioinf.org.uk/software/profit/). The side chain of amino acids with problems was fixed choosing the best rotamer browsing a rotamer library included in the program SPDBV [37], followed by intensive cycle of energy minimization, applied to a region about 10 Å around the changed amino acid [38, 39]. Further energy minimization of structures was done with the program NAMD [40], using the Amber99 force field [41], to a convergence criterion for the energy gradient of 0.005 kJ/mol. Final models were obtained after an equilibration of the system by a constrained molecular dynamics simulation. After an extensive energy minimization, models were stepwise heated to 300 K, and equilibrated for at least 500 ps at the final temperature. Backbone atoms were constrained by a harmonic force of 1 kJ/mol per Å$^2$ during the simulation. The time step of the simulations was 2 fs, non-bounded pairs were updated every 20 steps, and cut-off for the non-bounded interactions was set to 12 Å. The shake [42] procedure was employed to constrain all bonds connecting hydrogen atoms.

Table 1. Apparent dissociation constants ($K_D$) for different CFTR activators.

| Compound | WT | G551D | G1349D |
|---|---|---|---|
| Apigenin[(a)] | 3. 1 ± 0.6 (4) | 19.6 ± 6.1 (3) | – |
| Genistein[(a)] | 19.6 ± 2.5 (15) | 114.2 ± 12 (3) | 34.38 ± 2.21 (3) |
| UCCF-023[(b)] | 0.5 ± 0.2 (3) | – | – |
| UCCF-029[(b)] | 1.5 ± 0.5 (4) | 31.3 ± 3.5 (3) | 11.7 ± 3.1 (5) |
| UCCF-030[(b)] | 0.5 ± 0.1 (3) | 4.7 ± 1.3 (2) | – |
| UCCF-853[(b)] | 1.17 (1) | – | – |
| C02[(b)] | 3.2 ± 0.3 (2) | – | – |
| C03[(b)] | 1.2 (1) | 7.2 ± 3 (2) | – |
| Act01[(c)] | 0.4 ± 0.04 (5) | – | 0.6 ± 0.2 (3) |
| Act03[(c)] | 0.07 ± 0.02 (2) | – | – |
| Act04[(c)] | 0.4 ± 0.08 (4) | not active up to 20 µM | – |
| Act05[(c)] | 0.13 ± 0.01 (4) | not active up to 5 µM | – |
| Act09[(d)] | 1.95 ± 0.7 (3) | not active up to 50 µM | – |
| Act11[(d)] | 0.3 ± 0.08 (3) | not active up to 20 µM | – |
| Act12[(d)] | 1.9 ± 1.3 (3) | – | – |
| Act13[(d)] | 0.2 ± 0.03 (3) | not active up to 20 µM | – |
| Act14[(d)] | 0.2 ± 0.04 (2) | – | – |
| Act17[(d)] | 1.1 ± 0.5 (6) | – | – |

Data were obtained from measurements of Isc on FRT cell monolayers expressing WT or mutant (G551D or G1349D) CFTR. All cell monolayers were pre-stimulated with 20 µM CPTcAMP. Data represent mean ± SE, with the number of experiments in parentheses. Origin of the substances: [(a)] Sigma-Aldrich; [(b)] Asinex; [(c)] ChemDiv; [(d)] ChemBridge.

Structural parameters and prediction quality of the modeled structure were evaluated using the programs Whatif [43, 44] and Procheck [45] from the Biotech web server (biotech.ebi.ac.uk). Structures of CFTR activators were optimized by molecular mechanics, using the UFF method [46] implemented in ArgusLab (Planaria Software). Atomic partial charges and van der Waals radius were estimated with the Anterchamber module of Amber [47].

Rigid docking was done with a geometric recognition algorithm, implemented in the program Gramm [48]. The program performs an exhaustive six-dimensional search through the relative translations and rotations of a rigid ligand molecule. The prediction was done with parameters designed for high-resolution structure [48]. Flexible docking was done using the genetic algorithm implemented in the program Gold (Cambridge Crystallographic Data Centre, UK), using the ChemScore scoring method [49, 50]. This algorithm performs an automated docking with full acyclic ligand flexibility, partial cyclic ligand flexibility and partial protein flexibility in the neighborhood of the protein active site [51, 52].

The electrostatic contribution to the molecule interaction energy ($\Delta G_{Elec}$) was calculated using the generalized Born model [53, 54]. The non-polar (hydrophobic) contribution to the intermolecular energy was calculated as $\Delta G_{HB} = \alpha\ \Delta SASA + \gamma$ [55–57], where SASA is the solvent-accessible surface area, calculated with the program NAccess [58], $\alpha = 0.00226$ kJ/mol Å$^2$, and $\gamma = 3.84$ kJ/mol.

### Materials

Zeocin was from Invitrogen. Fetal bovine serum was from Gibco. Except when specified, all chemicals were purchased from Sigma. The chemical structure of the 18 CFTR activators tested is shown in figure 1. The identifications of the test compound series 'UCCF' [11, 59] and 'Act' [10] were kept as originally reported. The origin of compounds is indicated in table 1.

## Results

### Electrophysiology

We compared the effect of different CFTR activators on the WT and on mutations of the signature sequences of CFTR, the NBD1 mutant G551D, and the mirror NBD2 mutant G1349D. To this end, we used FRT cells stably transfected with CFTRs and measured on polarized epithelia the effect of activators as apical membrane short-circuit current (Isc) increase. After treating WT CFTR with different concentrations of the membrane-permeable cAMP analogue CPTcAMP, we obtained dose-response curves for genistein with a lower apparent dissociation constant ($K_D$) after higher levels of phosphorylation obtained by application of higher CPTcAMP concentration (fig. 2). For example, the fit of dose-response curves yielded apparent $K_D$s for genistein of 5.8±0.7 and 29.1±3.8 μM after stimulating cells with 100 and 10 μM CPTcAMP, respectively. To compare the effect of various CFTR activators on Isc, we used conditions as homogeneous as possible. Epithelia were always pre-stimulated with 20 μM CPTcAMP, a concentration that permitted successive activation of relatively high currents with CFTR activators on both WT and mutant CFTRs (fig. 3A).

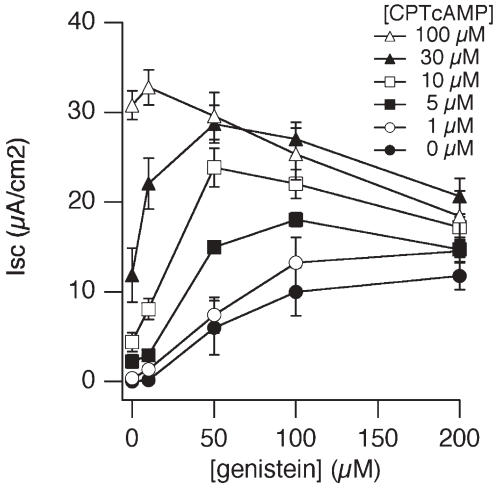


Figure 2. Effect of phosphorylation levels on the affinity of WT CFTR to activators. Dose-responses to genistein of WT-CFTR at different concentrations of CPTcAMP. The first point at 0 μM genistein is the response to CPTcAMP added to both hemichambers. The concentrations of CPTcAMP are indicated. Genistein was added only to the apical side. Each point is the mean of four to six experiments in different preparations and vertical bars represent the SE. Note the shift to the left of the activation curve with increasing CPTcAMP concentrations.

Our data indicated, as already observed in previous experiments [18], that the genistein dose-response curve on G551D epithelia was shifted to the right with respect to WT protein (fig. 3A, B). We found that genistein also caused an Isc increase on the G1349D mutant (fig. 3A). The dose-response curve for the G1349D mutant was shifted to the right with respect to WT cells, but to a lesser extent than that of G551D (fig. 3B). We examined the affinities of other CFTR activators, such as UCCF-029, recently identified by high-throughput screening, and the flavone apigenin. In all cases, the affinities for the G551D mutant were significantly shifted to the right with respect to the WT protein, and the affinities for G1349D were in-between (fig. 3C, D). Table 1 lists apparent $K_D$s for 18 compounds (see fig. 1) on the three CFTR-proteins obtained in similar experiments.

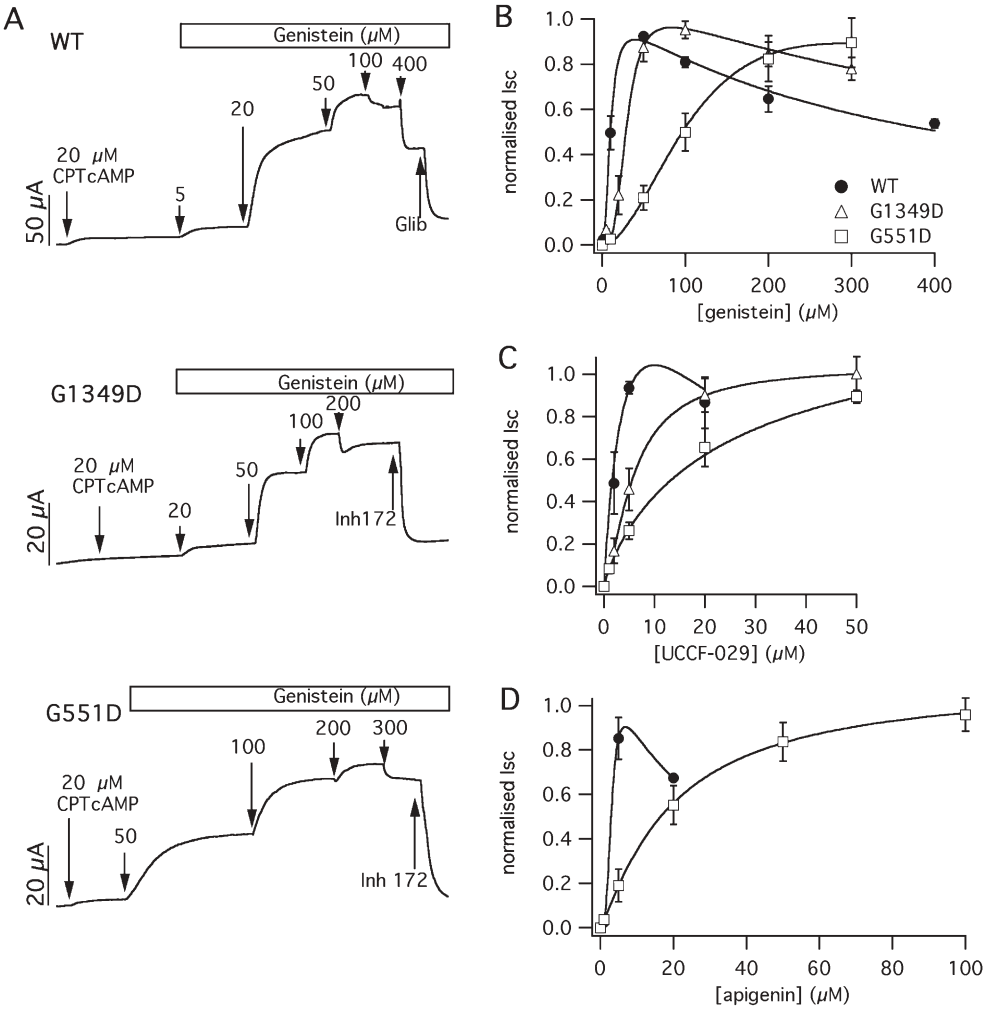


Figure 3. Effect of different CFTR activators on polarized epithelial preparations expressing WT or CFTR mutants (G1349D and G551D). (*A*) Short-circuit currents measured on FRT permeabilized epithelia expressing WT or mutant CFTR. Increasing concentrations of genistein on the apical membrane after phosphorylation of the channel with 20 μM CPTcAMP cause a dose-dependent increase in current. Note that the lowest concentration that inhibited CFTR currents was 100 μM for WT and 200 μM for G1349D, while 200 μM still stimulated G551D. (*B–D*) Normalized dose-response relationships of FRT cells expressing WT (closed circles), G1349D (open triangles) and G551D (open squares) CFTR to genistein (*B*), UCCF-029 (*C*), and apigenin (*D*). The affinity shift in the mutants was extremely reproducible in all preparations. The apparent $K_D$ values are indicated in table 1. Symbols are the mean ± SE of 3–13 measurements with a single compound in different preparations.

**NBD model**

Modeling of the human NBDs was done by homology to murine NBD1. The sequences corresponding to the NBDs of the human CFTR (SwissProt accession number P13569) were aligned to the sequence of murine NBD1 (PDB ids 1R1, 1R0Z, 1R0Y, 1R0X, 1R0W and 1Q3H) solved by X-ray crystallography [20]. The crystalline segment of murine NBD1 was defined from residue 390 to residue 660. The human counterpart, defined in the same residue interval (390–660), had a homology of 96.3%, and 79% identity. Human NBD2, defined from residues 1180 to 1456, has a lower homology to murine NBD1 (56%), and 25% identity (see fig. 4). The homology between murine NBD1 and both human NBDs is largely above the requirement for a safe structural prediction by molecular homology (≥35%) [60]. Resulting NBD monomer structures were extensively minimized before proceeding to the next modeling step.

Dimerization of NBDs seems to be a common feature of the ABC family, either in prokaryotes with functional proteins assembled by TMD and NBD domains encoded by independent polypeptides, or in some prokaryotes and most eukaryotes where ABC transporters are formed by a unique polypeptide with two TMD-NBD halves [2]. Dimerization of the NBDs is required for ATP binding and hydrolysis in all ABC transporters [2, 24, 61]. Several different dimeric conformations have been obtained by crystallization of bacterial NBDs [for a review, see ref.

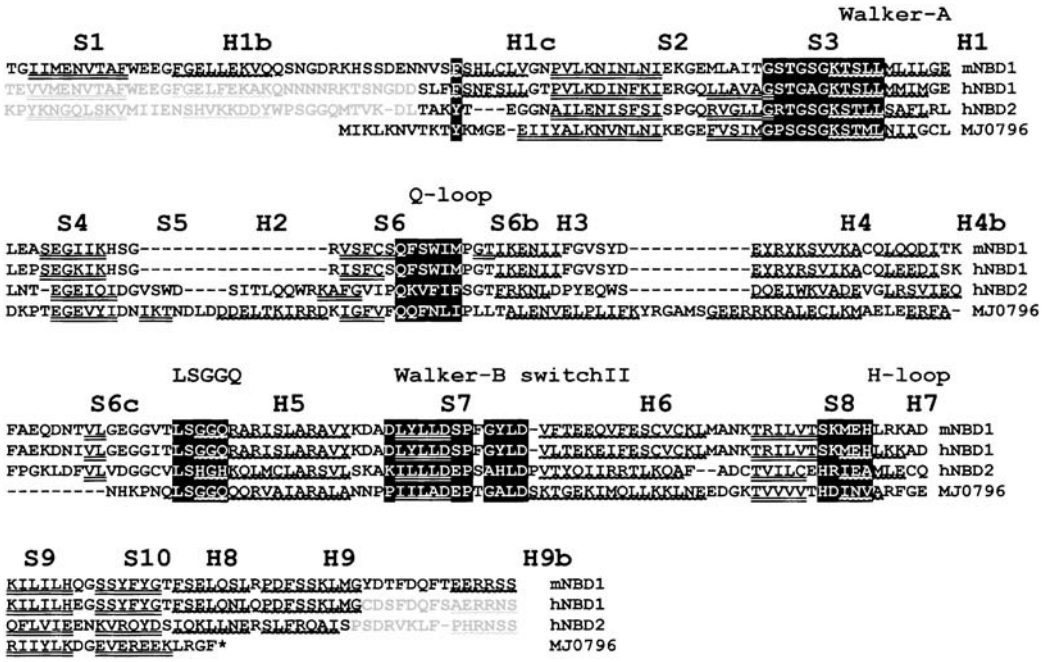


Figure 4. Alignment of the primary structures of (murine) mNBD1, (human) hNBD2 and hNBD2, and the NBD of the MJ0796 putative ABC transporter from the archeobacterium *M. jannaschi*. Helices (H) are indicated with wavy underline, and sheets (S) with double underlining. Secondary-structure regions were defined by the program DSSP [82], using the crystallographic structure of mNBD1 and the MJ0796 NBD and the homology models of hNBDs. Numeration of helices and sheets was done according to Lewis et al. [20]. Conserved NBD signature sequences are indicated by black background. Gray characters indicate regions of hNBDs excluded from the dimeric model.

24]. Among them, the head-to-tail conformation is most consistent with ATP hydrolysis [25, 62–66]. Hence, we have hypothesized that the functional conformation of CFTR NBDs is dimeric in the head-to-tail conformation. Therefore, we used the structure of the putative ABC transporter from *M. jannaschi,* MJ0796 (PDB entry 1L2T), as a template for modeling the CFTR NBD dimer [26, 27]. The structure of the MJ0796 NBD dimer was obtained from a mutant where a glutamate in the C terminal of the Walker-B motif was substituted by glutamine, resulting in a phenotype that binds ATP but does not hydrolyze it. Consequently, the solved structure contains two ATP molecules in its binding site [26]. Models of human NBD1 and NBD2 were aligned to MJ0796 (see fig. 4), taking into account the conserved motifs of the NBDs and the secondary-structure conservation. Successively, NBD1 and NBD2 were fitted to the MJ0796 dimer. No significant differences in the dimeric CFTR NBDs were found by fitting NBD1 and NBD2 into chains A and B of the MJ0796 structure, respectively, or B and A, respectively. Data presented here correspond to the fitting of NBD1 and NBD2 into chains A and B, respectively. Two ATP molecules were added to the model in positions equivalent to those of the nucleotide in the MJ0796 dimer.

Fitting of human CFTR NBD1 and NBD2 into the MJ0796 dimer produced two clash regions, as observed by Lewis and collaborators when they attempted to construct a murine NBD1 dimer [20]. The N terminal of each NBD forms a loop that occupies the same place as the LSGGQ signature of the complementary NBD. The second conflict is found in the C-terminal regions, where the loops between helices H9 and H9b are superposed. The incompatibility of the N terminal with the NBD dimer model should be important, as it relates to the ATP-binding sites. In the crystalline murine NBD1 structure, ATP is bound between the Walker-A domain and the N terminal of the same polypeptide [20]. We propose that this position of the N terminal is artifactual, as NBD1 in the crystal does not form dimers. One possibility is that the monomeric crystal 'forced' the position of the N terminal to substitute the missing LSGGQ signature of the complementary NBD to complete the ATP-binding site. Indeed, when ATP is removed from the model and a free molecular dynamic simulation is applied, the N-terminal region acquires a very high mobility, and different conformations can be observed (data not shown). The N-terminal strand and loop region that is in conflict with the NBD-NBD association may be important for CFTR function, as it contains some potential protein kinase A (PKA) phosphorylation sites. This region has been suggested to bridge the NBD and the transmembrane domain [66–68]. The C-terminal helix, which corresponds to the beginning of the regulatory domain, may also be involved in PKA regulation of CFTR. A second possibility is that a conformational change occurring upon 'dimerization'

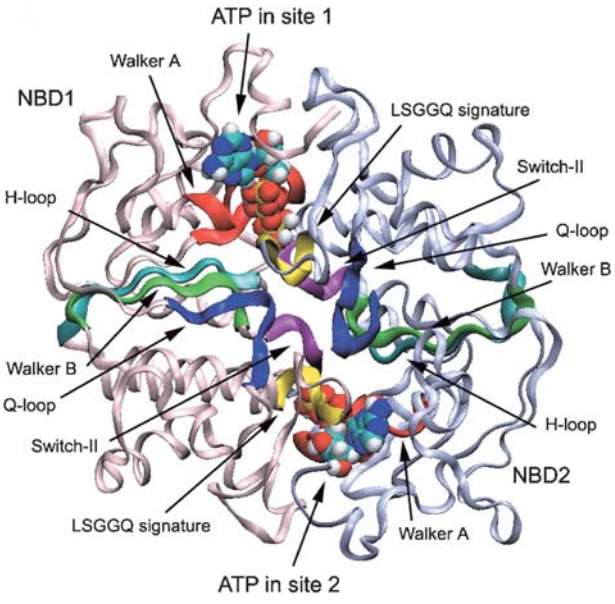


Figure 5. Dimeric model of the human CFTR NBDs. NBD1 (pink) and NBD2 (blue), represented as ribbons, are in the 'head-to-tail' dimeric configuration. ATP molecules, bound in their sites at the NBD-NDB interface, are represented as van der Waals spheres. Conserved regions of each NBD are indicated in the figure.

may move out clashing regions.These clashing segments might also be displaced when phosphorylated on sites in the S1-S2 loop and in the H9b helix, promoting and maintaining NBD1-NBD2 association [20]. This is in agreement with the poor definition of the structure of H1b and S2 in the murine NBD1 template. Hence, we removed the first 38 residues from the NBD1 model and the first 37 residues from the NBD2 model. The resulting dimer shows that the ATP-binding sites are formed by the Walker-A domain of one NBD, and the LSGGQ signature of the complementary NBD (fig. 5).

After construction of the NBD dimer, including the two ATP molecules and equilibration to 300 K by molecular dynamics, structural parameters of the model were checked by the programs Procheck and Whatif. The Ramachandran plot indicated that only five residues (1.3%, excluding glycine and proline) lie in disallowed regions. As expected for well-minimized models, no bad contacts or clashes were present, and a small value (3.3 kJ/mol) was estimated for the standard deviation of the overall hydrogen bond energy. Analysis for distortion of the backbone, $\chi$ angles of side chains, atomic volume analysis and molecule packing yielded scoring factors corresponding to allowed conformations, and distributions of bond length and angles were within the accepted values for protein structures. The overall evaluation indicated that the model of CFTR NBDs ranked as an acceptable structure.

The final model, containing the fingerprint regions of the ABC transporters, is represented in figure 5. Of interest is that all the conserved domains contribute to form the surface of contact between the two NBDs (fig. 5). The significant reduction of the SASA (–3117 Å$^2$, ≈16% of the total SASA) by dimerization of NBD1-NBD2 indicates that hydrophobic energy ($\Delta G_{HB}$ = –66.6 kJ/mol) plays an important role in the inter-domain interactions. The electrostatic energy contribution to the inter-domain interactions also seems to favor the dimerization ($\Delta G_{Elec}$ = –17.2 kJ/mol). The dimer is well stabilized by 28 hydrogen bonds, 22 of them involving residues of the Walker-A motif near to ATP-binding sites. Indeed, when $\Delta G_{HB}$ and $\Delta G_{Elec}$ are calculated in the presence of ATP, these two terms become more negative (–98.4 kJ/mol and –23.9 kJ/mol respectively). This could indicate that the presence of ATP stabilized the NBD1-NBD2 dimer (table 2).

ATP-binding sites in human CFTR NBDs occur in the mutual interface of the dimer conformation, in which two ATP molecules are sandwiched between the Walker-A motif of one subunit and the C-loop motif of the other subunit. Binding sites are named site 1 (Walker-A from NBD1, and LSGGQ signature and switch-II domains from NBD2) and site 2 (Walker-A from NBD2, and LSGGQ signature and switch-II domains from NBD1). When ATP is bound in the NBDs, it is stabilized by hydrogen bonds to nine residues in site 1 and to eight residues in site 2. To compare the properties of ATP binding in each site, we attempted an empirical calculation of free energy of binding ($\Delta G_{bind}$) to the NBD dimer, including the electrostatic, the hydrophobic and entropic energy terms [69]. The difference of $\Delta G_{bind}$ in site 1 and $\Delta G_{bind}$ in site 2, $\Delta\Delta G_{bind}$, is –2.78 kJ/mol, consistent with a different ATP affinity at the two sites, and corresponding to a higher affinity for ATP in site 1 (table 3) [28, 70–72].

Molecular models of mutants contain several differences compared to the WT model. The two mutations studied, G551D and G1349D, are located in the LSGGQ signature of NBD1 and NBD2, respectively. Neither of the mutated

Table 2. Hydrophobic ($\Delta G_{HB}$) and electrostatic ($\Delta G_{elec}$) contributions to interaction between NBD1 and NBD2 from WT and the mutants G551D and G1349D.

| | WT | G551D | G1349D |
|---|---|---|---|
| NBD1 + NBD2 | | | |
| $\Delta G_{HB}$ (kJ/mol) | –66.1 | –68.4 | –69.3 |
| $\Delta G_{elec}$ (kJ/mol) | –17.2 | –12.5 | –13.1 |
| NBD1 + NBD2 + 2 ATP | | | |
| $\Delta G_{HB}$ (kJ/mol) | –98.4 | –98.44 | –101.05 |
| $\Delta G_{elec}$ (kJ/mol) | –28.9 | –23.3 | –24.3 |

Data were calculated from the interaction of NBDs in the absence of ATP, NBD1-NBD2, and from NBDs interacting in the presence of ATP, NBD1-NBD2-2 ATP.

Table 3. Comparison of the binding free energy differences, $\Delta G_{bind}$ estimated for ATP-binding sites 1 and 2, for WT and the mutants G551D and G1349D of human CFTR.

| | WT | WT-G551D $\Delta\Delta G_{bind}$ (kJ/mol) | WT-G1349D $\Delta\Delta G_{bind}$ (kJ/mol) |
|---|---|---|---|
| Site 1 | | 1.83 | 11.06 |
| Site 2 | | 12.98 | 3.3 |
| Site1-site 2 | –2.78 | 13.92 | –4.99 |

Changes are expressed as differences in $\Delta G_{bind}$ ($\Delta\Delta G_{bind}$), calculated at different conditions.

residues is directly involved in the NBD-NBD interaction, but the mutations modify several hydrogen bonds in the contact regions near the binding sites. The hydrophobic contribution to the interaction energy is slightly improved in the mutants ($\Delta G_{HB}$ = –68.4 kJ/mol for G551D, and $\Delta G_{HB}$ = –69.3 kJ/mol for G1349D), but electrostatic terms of energy are significantly increased ($\Delta G_{Elec}$ = –12.5 kJ/mol for mutant G551D, and $\Delta G_{Elec}$ = –13.1 kJ/mol for mutant G1349D), with a net increase in the interaction energy of 2.9 kJ/mol and 1.4 kJ/mol for G551D and G1349D, respectively (table 2). This would indicate a possible general destabilization of the NBD-NBD dimer by these mutations. Major modifications are observed in the ATP-binding sites of the mutants (table 3). For mutant G551D, there is a reduction in the affinity for ATP in site 2 ($\Delta\Delta G_{bind}$ = 13 kJ/mol), but ATP-binding site 1 is almost unaffected ($\Delta\Delta G_{bind}$ = 1.83 kJ/mol). Conversely, for mutant G1349D, the affinity for ATP is reduced in site 1 ($\Delta\Delta G_{bind}$ = 11.1 kJ/mol), with a smaller effect on site 2 ($\Delta\Delta G_{bind}$ = 3.3 kJ/mol).

**CFTR activators docking**

A geometrical docking algorithm implemented in the program Gramm undertook initial prediction of possible binding sites for CFTR activators in the NBD dimer. It performs an exhaustive search of configurations that maximize the contact area of the ligand in the NBD model surface [48]. This initial step was done docking two compounds, genistein and apigenin, to the WT NBD1-NBD2 model, including two bound ATP molecules. The 20,000 configurations obtained by the docking were considered for the analysis. To search the possible binding sites, the NBD dimer was divided by a 4-Å grid, and an empirical binding energy term, calculated as the sum of raw electrostatic and hydrophobic energy contributions, was calculated for each cell of the grid. The probability of forming a binding site was calculated as proportional to the exponential of the empirical binding energy term. The analysis yielded several minima for each ligand. We selected three positions, named site 1, site 2 and site 3, which were shared by the two ligands tested and displayed the lowest energy values. Results obtained for genistein are shown in figure 6. The color scale of polypeptide residues in the figure represents the average empirical binding energy for the ligands in the grid cell near each amino acid. Observe the three distinct positions of the genistein baricenter, indicated by small green spheres. The putative binding site 1 includes the N terminal of sheet S6, helix H5 and the loop between helices H3 and H4 of NBD2. Site 2 is a gap between NBD1 and NBD2, which includes residues of the Q-loop of NBD2, and Q-loop, part of the LSGGQ signature and switch-II of NBD1. Site 3 is near to the ATP bound in site 1, the C terminal of the LSGGQ signature of NBD2, and Q-loop and the N terminal of the LSGGQ signature of NBD1.

Experimental data on affinity obtained from LSGGQ signature mutants indicate that position 551 strongly affects the apparent dissociation constant of most CFTR activators, while it is less affected by a mutation in position 1349 (see table 1). These observations favor the choice of site 2 and 3, as both putative binding sites for the CFTR activators are near to the LSGGQ signatures of both NBDs. Putative site 1 does not seem to involve any of the LSGGQ signatures. To decide between putative sites 2 and 3, we compared the apparent dissociation constant evaluated experimentally and the empirical energy interaction obtained from the model. Calculations were also done for putative binding site 1 for comparison. The apparent dissociation constant $K_D$ is the result of a series of events including the process of binding the CFTR

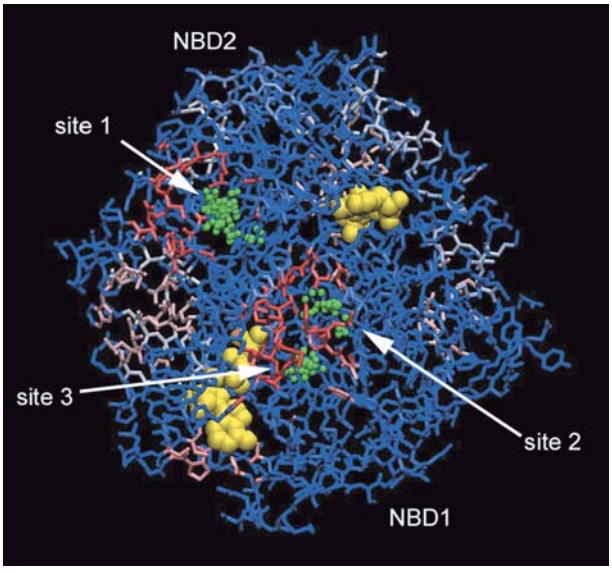


Figure 6. Putative binding sites for the CFTR activators at the NBDs. The structure of the NBDs is draw with a color scale (blue-white-red) proportional to the probability of forming a binding site (proportional to the exponential of the mean empirical binding energy term). Green spheres indicate the baricenter position of the ligand (genistein) near to each high-probability (low-energy) region. ATP molecules are represented as yellow space-fill.

activator and the conformational changes that cause channel opening. Here we simply hypothesized that differences in the molecular structure of the CFTR activators, or modifications of their binding site, would change primarily the binding energy of these substances. Consequently, the main contribution to the apparent dissociation constant changes is due to these local changes in the binding affinity of the CFTR activators. Hence, we calculated 'the free energy' from the apparent dissociation constants estimated experimentally, $K_D$, as $\Delta G_{exper} = RT \ln(K_D/1M)$, where R is the gas constant and T is absolute temperature.

We attempted the docking of the 18 CFTR activators, for which we have studied the apparent dissociation constant, to the WT NBD dimer including two ATP molecules. Docking to mutant models was also calculated for those compounds that were studied experimentally. We used a flexible docking method using the genetic algorithm implemented in the program GOLD. Scoring of the possible conformations was done according to ChemScore. Docking was attempted for all three putative binding sites, starting in the baricenter of each site, and exploring a region with a radius of 15 Å. We repeated the procedure 100 times, with 100,000 permutations of an initial 100 member population. The advantage of ChemScore is that it also provides an empirical calculation of the binding free energy, $\Delta G_{model}$ [50]. The mean value of $\Delta G_{model}$ from 100 docking runs for each ligand at each putative binding site was compared with $\Delta G_{exper}$ obtained from experimental data. Comparison of experimental and theoretical free energies is shown in figure 7. Data obtained for all three putative binding sites are shown in the inset. The Pearson correlation coefficient of $\Delta G_{model}$ versus $\Delta G_{exper}$ yielded values of –0.07 and –0.46 for the putative sites 1 and 3, respectively. The regression lines for site 1 had a slope non-different from zero, and for site 3, the slope was negative. The slope values and the low Pearson correlation coefficient indicate that $\Delta G_{model}$ calculated from the docking results in the putative sites 1 and 3 is not correlated with the experimental results. Conversely, the slope of the regression line of $\Delta G_{model}$ versus $\Delta G_{exper}$ for the site 2 was 0.71±0.09, and the Pearson correlation coefficient 0.83, indicating a good correlation. Thus, values of $\Delta G_{model}$ estimated for different ligand-NBD dimer complexes would allow prediction of the affinity of CFTR activators. As an example, we calculated the affinity of the compound UCCF339 [59] for the WT CFTR. The $\Delta G_{model}$ estimated from the docking of this substance to the NBD dimer model was –28.1 kJ/mol, which corresponds to $\Delta G_{exper}$ of –31.3 kJ/mol. This binding energy corresponds to a dissociation constant of 3.6 μM, not very different from the $K_D$ obtained experimentally (1.7 μM) by fluorescence measurements [59]. Similarly, we estimated the $K_D$ for some of the compounds for which the affinity for the mutant G551D was too low

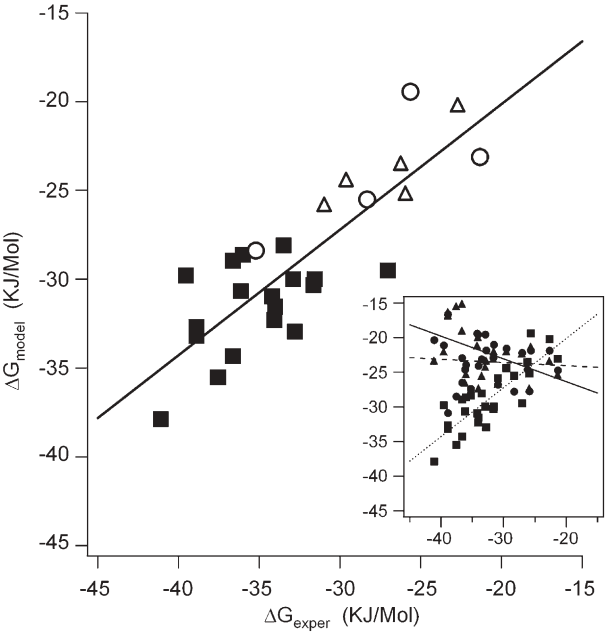


Figure 7. Correlation between the binding free energy difference calculated from experimental measures of the apparent dissociation constant, $\Delta G_{exper}$, and from the docking theoretical models, $\Delta G_{model}$. Filled symbols represent data obtained docking the CFTR-activator to the WT model, open triangles are from G551D, and open circles are from G1349D. A continuous line represents the linear fit. The inset of the figure shows the fitting of data for the three putative binding sites 1 (solid circles), 2 (solid squares) and 3 (solid triangles). Fitting results for putative site 1 yielded: intercept a = 25.1±4.1 kJ/Mol, slope b = –0.05±0.13, and Pearson's correlation coefficient, r = –0.07 (dashed line); for site 2: a = –6.0±3.0, b = 0.71±0.09, r = 0.83 (continuous line); for site 3: a = –32.9±4.5, b = –0.33±0.14, r = –0.46 (dotted line).

to be measured experimentally (see table 1). For example, for Act05, Act09 and Act11 we obtained $\Delta G_{model}$ of –22.2, –22.4 and –13.3 kJ/mol, respectively, corresponding to apparent $K_D$ values of 103 μM, 93 μM and 15 mM, respectively.

We conclude that, in our model, the region identified as putative site 2 has the properties to be considered the possible binding site for the CFTR activators that bind to the NBD dimer. As mentioned before, site 2 is located in a cavity at the interface between NBD1 and NBD2 (see fig. 6). Part of the ligand is inserted in a cavity within NBD1, and the interface surface of NBD2 (fig 6). The CFTR activator bound in site 2 forms close hydrophobic and hydrogen bond contacts with Walker-A, LSGGQ signature and Walker-B domains of NBD1, and to a lesser extent with the LSGGQ signature of NBD2 (fig. 8). Similar compounds seem to accommodate in the binding site 2 with the same orientation (fig. 8), indicating that a more careful comparative analysis of the conformation of different ligands will allow good pharmacophore characterization of the CFTR activators.

## Discussion

We recently studied the effect of some CFTR activators on cells expressing either the WT or G551D mutant CFTR [18]. We found that the genistein dose-response curve in G551D cells was shifted with respect to WT CFTR so that higher concentrations were required to observe activation. This result strongly indicated that the G551D mutation is near a binding site for genistein. Although various studies have reported the effects of different CFTR openers, each has usually dealt with a single compound in a different cell preparation using different protein mutants and with different assays and conditions (single-channel and whole-cell $Cl^-$ currents, transepithelial $Cl^-$ transport, $I^-$ efflux, room temperature and 37 °C, etc). This lack of experimental consistency makes it difficult to compare the results obtained in the different studies. This is important, because we and other authors have observed that the apparent affinities of several compounds depend on the phosphorylation status of the protein [34, 73].

Here we studied the pharmacological properties of a series of 18 different CFTR activators. Two of them, genistein and apigenin, have been extensively characterized in the literature, while the other 16 are the results of a previous high-throughput screening of chemical libraries [10, 11, 59]. We evaluated the apparent dissociation constant of the CFTR activators, $K_D$, for the activatory binding site from dose-response curves obtained by measuring the Isc increase upon application of the activator. We defined $K_D$ as the concentration that produces half the maximum increase in current. This definition, independent of the model to interpret the system, would represent an equilibrium condition. Experiments were done with conditions as homogeneous as possible, to permit comparison of results between different CFTR activators and from data obtained on WT and mutant CFTR. The first important observation is that mutations in the NBDs lead to a reduction in the affinity of the CFTR activators. Similar results have already been reported for genistein on the mutation G551D [18] and for genistein and two benzimidazolone analogs with the mutation dF508 [19]. Now, we extend these observation to five substances tested on mutant G551D and three tested on mutant G1349D. Interestingly, there is a decrease of affinity for every CFTR activator tested on the mutants, the reduction being more marked for mutant G551D than for mutant G1349D (table 1). These data are in good agreement with the hypothesis that NBDs are a target for CFTR activators [12, 14–16]. Therefore, we further elaborated this hypothesis by developing a molecular model of the CFTR NBDs, and attempting the docking of CFTR activators to the model.

The affinity of CFTR activators was dependent on CPTcAMP concentration in the WT but not in the mutants (data not shown). The choice of 20 μM CPTcAMP was arbitrary, to maximize the current measured in mutant CFTRs which was negligible in the absence of CPTcAMP. Affinities determined at zero CPTcAMP may have yielded higher apparent $K_D$ values for the WT and, hence, less negative $\Delta G_{exper}$ values, resulting in an even stronger correlation between $\Delta G_{model}$ and $\Delta G_{exper}$. However, we assume that although WT affinities measured at 20 μM CPTcAMP may be slightly higher than in the absence of CPTcAMP, the error introduced is small enough to be disregarded within the context of the whole study.

Molecular modeling of CFTR-NBDs is facilitated by the wide biological distribution of ABC transporter proteins. ABC transporters share the same basic architecture, with two NBDs, which have relatively well-conserved topological motifs among all members of the family [24, 32, 74–76]. Moreover, data on the molecular structure of the murine CFTR NBD1 have allowed modeling of the human counterparts to be undertaken with a good confidence level. ABC transporter mechanisms are strongly linked to ATP binding (and in most cases, hydrolysis) to the NBDs. For CFTR also, gating of the chloride channel has been shown to depend on binding of ATP in the NBDs [4, 5]. A well-supported model for the CFTR activation mechanism proposes the channel gating to be coupled to NBD dimerization [16, 77]. As binding of ATP favors the dimerization of NBDs in various ABC transporters [26], a similar mechanism in CFTR would explain in part the coupling between ATP binding and channel gating [77]. Therefore, we presume that the functional active configuration of the CFTR NBDs is dimeric. By comparison with other ABC transporter proteins, the most probable configuration of the NBD dimer would be the 'head-to-tail' configuration, where the Walker-A domain of each NBD interacts with the LSGGQ signature of its counterpart [24, 61]. The validity of this configuration as functional has been confirmed for NBDs of Rad50 [25], HisP[3], MalFGK2 [78], P-gp [22] and MJ0796 [26, 79].

We modeled the human NBD1-NBD2 dimer using the structure of MJ0796 as a template. To solve the structure of MJ0796 NBDs, mutation E171Q, which abolishes the hydrolysis of the bound nucleotide, was introduced in the polypeptide [26, 27]. It allowed crystallization of the MJ0796 NBD dimer with two ATP molecules bound in their sites. Thus, we used in our model a relative position of ATP similar to that of MJ0796. Similar models, but based entirely on the MJ0796 structure, have been proposed previously [76, 80]. These models share the same general properties as those shown in the model presented here.

The structures of CFTR NBD1 and NBD2 are characterized by a strong asymmetry. Indeed, identity between NBD1 and NBD2 (27%) is lower than the identity of both CFTR NBDs and an NBD of another member of the ABC transporter family (for example, with NBDs of human

multidrug resistance protein-1, there is an identity of 42% and 40% for NBD1 and NBD2, respectively). ATP-binding sites are identified in the NBD-NBD interface, with a contribution of residues from both domains (fig. 5). One functional consequence of the structural asymmetry is a large difference between the two ATP-binding sites. Biochemical evidence suggests that ATP site 1 is a site of slow turnover, whereas site 2 is a catalytically more active site [28, 70–72]. Thus, ATP binding at both sites would drive opening, while unbinding at site 2 would drive closure of the CFTR $Cl^-$ channel [4, 71, 77]. From the estimations of the binding free energy difference for each ATP site, we found a $\Delta\Delta G_{bind}$ of –2.8 kJ/mol that is consistent with a higher affinity of ATP for site 2. Mutations analyzed here are in the LSGGQ signature of each NBD. Consequently, we expect that these mutations would affect the ATP binding, and this effect would be the primary cause for the strong current reduction of cells expressing CFTRs carrying these mutations. Indeed, comparing the empirical estimations of the binding free energy difference, we found that $\Delta\Delta G_{bind}$ for mutant G551D is consistent with a strong reduction in ATP affinity at site 2, where the mutated residue is more directly involved, and a smaller reduction in ATP affinity for site 1. Similarly, as site 1 is more directly affected by mutation G1349D, a more severe reduction in ATP affinity is observed than in site 2. These results are in agreement with direct measurements of ATP binding done in NBDs of multidrug resistance protein-1 [31], where mutations G771D and G1433D of LSGGQ signatures, equivalent to G551D and G1349D in CFTR NBDs, produced similar effects on ATP-NBD interactions.

We evaluated empirically two main energetic contributions to interactions to the NBD-NBD dimer, hydrophobic, $\Delta G_{HB}$, and electrostatic, $\Delta G_{ELEC}$. Both energetic contributions clearly indicate that dimerization is an energetically favorable conformation. Dimerization seems to be largely stabilized by a series of hydrogen bonds between NBD1 and NBD2. Interestingly, most hydrogen bonds seem to occur between Walker-A of one domain and the LSGGQ signature of the other NBD, where the ATP-binding site is located. This may imply that ATP binding would play an important role in the dimerization of CFTR NBDs [77]. Indeed, both electrostatic and hydrophobic contributions to the NBD1-NBD2 interaction are strongly improved by the presence of ATP in the dimer (table 2). This is consistent with the idea that ATP binding favors the dimerization that, in turn, would be coupled with the channel gating [16, 77]. Docking of CFTR activators was done with the hypothesis that the binding site for these substances that activate

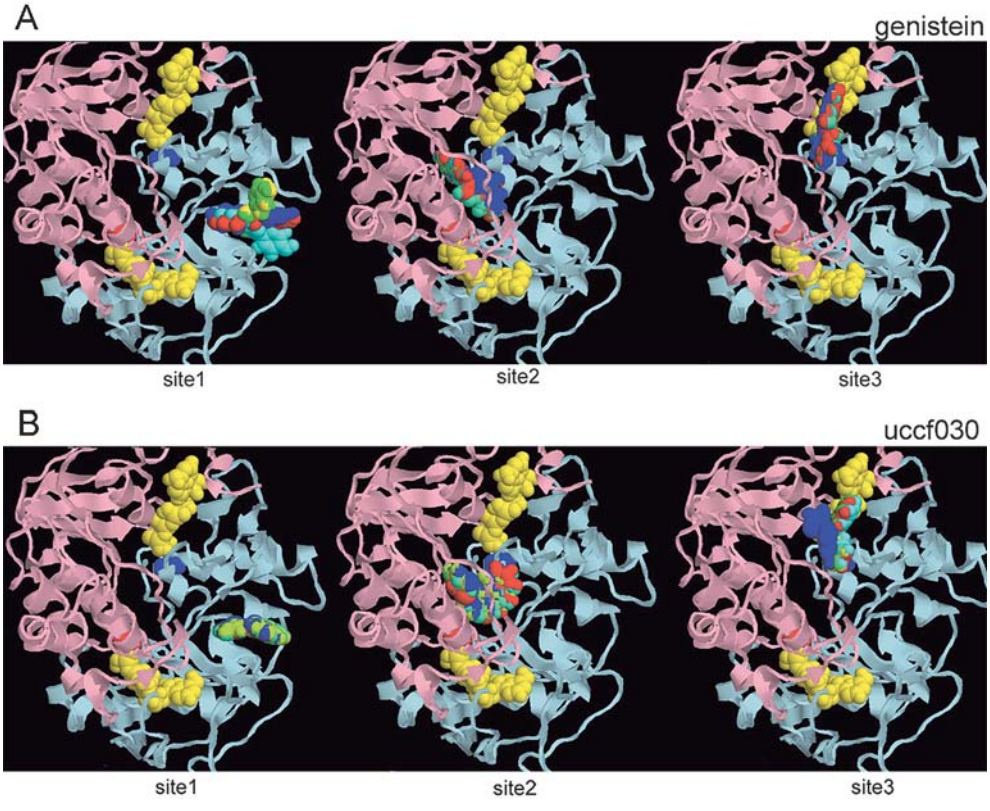


Figure 8. Docking of genistein (*A*) and UCCF030 (*B*) to the three putative binding sites. Positions of five conformations for each ligand are represented as space-fills. NBD1 and NBD2 are represented as cartoons colored pink and light blue, respectively. ATP molecules are represented as yellow space-fills.

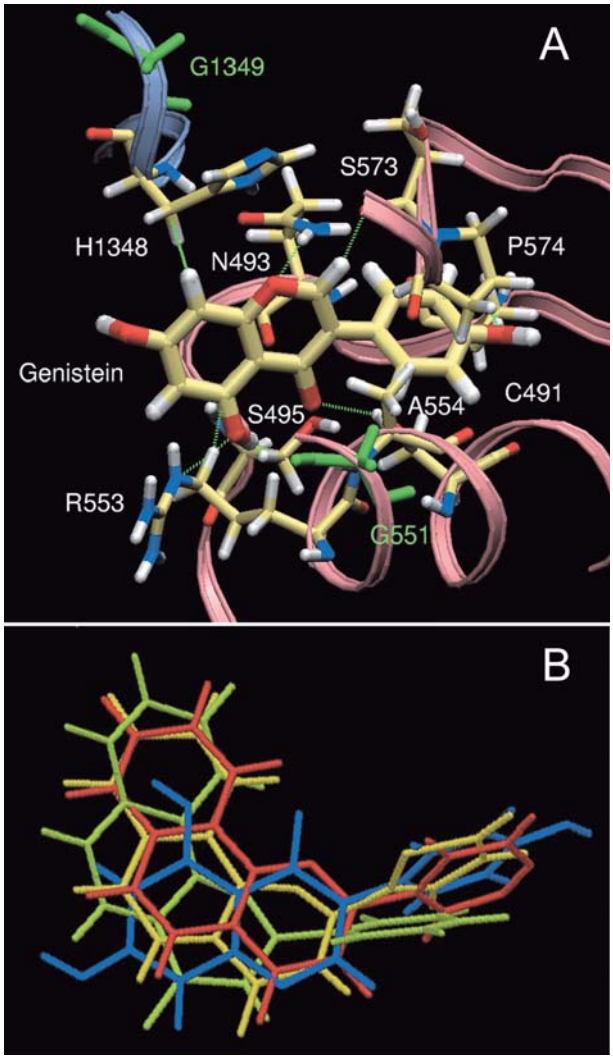


Figure 9. (*A*) Genistein molecule in the putative binding site 2. NBD1 and NBD2 are represented as pink and light-blue ribbons, respectively. Residues with high probability (>56%) to form hydrogen bonds with the ligand are indicated. Positions of mutations (G551 and G1349) are indicated in green. Observe that these residues do not interact directly with the ligands, but the consecutive amino acid. (*B*) Mean orientation of genistein (blue), UCCF023 (green), UCCF029 (red) and UCCF030 (cyan) in binding site 2. Observe the good superposition of different molecules.

the $Cl^-$ currents may be located in the NBDs. We proceeded with a blind rigid-docking strategy, generating a considerable number of possibilites (20,000) to be evaluated. We used a rough approximation to the energy of each configuration obtained, to reduce the calculation times, and have a consistently high number of individual configurations to be considered in the statistics. This analysis resulted in three 'hot spots' with low interaction energy, two of which, namely site 2 and site 3, being topologically compatible with the experimental results (fig. 6). Indeed, they are near the two LSGGQ signatures, positions where mutations modify the CFTR activator affinity. Thus, the subsequent analysis was done with the two putative sites, 2 and 3, to identify which was the most probable CFTR activator-binding site, and also in site 1 as a comparison for negative results.

The goodness of the correlation between $\Delta G_{exper}$ and $\Delta G_{model}$ will depend on having a wide enough range of affinities to make a good regression line. However, the CFTR activators that we could study have a small range of dissociation constants. To overcome this inconvenience, we included the $\Delta G_{exper}$ and $\Delta G_{model}$ data obtained from CFTR mutants. This can be justified by the fact that the apparent dissociation constant measured on mutants would depend mostly on a local interaction of the CFTR activator with the NBDs, and not on the intrinsic properties of gating of the channel that were modified by the mutation. Even with this assumption, we were very fortunate to find that, at least one of these putative sites, site 2, showed a good correlation between $\Delta G_{exper}$, calculated from the dissociation constants measured electrophysiologically (table 1), and $\Delta G_{model}$, estimated from the flexible docking runs for CFTR activators at each putative binding site. The other two putative binding sites showed a non-significant correlation and an almost-zero slope for the fit of $\Delta G_{model}$ versus $\Delta G_{exper}$ (see fig. 7). We used the advantage of estimation of the docking score based on ChemScore implemented in the program Gold, for calculation of $\Delta G_{model}$. ChemScore is based on a parameterized calculation of the binding free energy that has proven to be quite consistent for homogeneous systems [50, 81]. The remarkably good correlation coefficient of the fitting shown in figure 7 for docking in the putative site 2 strongly suggests that it is the binding site for CFTR activators.

The binding site for the CFTR activators hypothesized here is located in the interface of the NBD dimer, strongly interacting with NBD1, and to a lesser extent with NBD2 (figs. 8, 9). This position is consistent with the dimerization of NBDs as a step for CFTR activation [16, 77]. As suggested by Hwang and collaborators [16], when a CFTR activator binds to its site in the NBD interface, it would stabilize the dimer, increasing the activity periods of CFTR, resulting in an increase in channel-open probability, with a consequent increase in $Cl^-$ transport. At the moment, we have no direct evidence for this hypothesis, but it can be considered an interesting working hypothesis for further investigations. Of interest will be to examine whether CFTR activator dissociation constants can be modified by mutations around the proposed binding site, where channels express with measurable activities. Similarly, a further docking trial, with new analog of known affinities, would be important to identify the pharmacophore of the CFTR activators. The model presented here is supported by several experimental observations. Its predictive power, including the effect of two CF-related mutations, indicates that it may be a good starting point for in silico screening of potential CFTR activators.

*Acknowledgements*. This work was supported by the Italian Cystic Fibrosis Research Foundation and FISR-MIUR, Italy. O. Z.-M. was partially supported by Italian FIRB_PRIME funds.

1 Riordan J. R., Rommens, J. M. Kerem B., Alon N., Rozmahel R., Grzelczak Z. et al. (1989) Identification of the cystic fibrosis gene: cloning and characterization of complementary DNA. Science **245:** 1066–1073
2 Higgins C. F. (2001) ABC transporters: physiology, structure and mechanismman overview. Res. Microbiol. **152:** 205–210
3 Jones P. M. and George A. M. (2002) Mechanism of ABC transporters: molecular dynamics simulation of a well characterized nucleotide-binding subunit. Proc. Natl. Acad. Sci. USA **99:** 12639–12644
4 Gadsby, D. C. and Nairn, A. C. (1999) Control of CFTR channel gating by phosphorylation and nucleotide hydrolysis. Physiol Rev. **79:** S77–S107
5 Sheppard D. N. and Welsh M. J. (1999) Structure and function of the CFTR chloride channel. Physiol. Rev. **79:** S23–S45
6 Hwang T. C. and Sheppard D. N. (1999) Molecular pharmacology of the CFTR Cl-channel. Trends Pharmacol. Sci. **20:** 448–453
7 Cohen B. E., Lee G., Jacobson K. A., Kim Y. C., Huang Z., Sorscher E. J. et al. (1997) 8-Cyclopentyl-1,3-dipropylxanthine and other xanthines differentially bind to the wild-type and delta F508 first nucleotide binding fold (NBF-1) domains of the cystic fibrosis transmembrane conductance regulator. Biochemistry **36:** 6455–6461
8 Weinreich F., Wood P. G., Riordan J. R. and Nagel G. (1997) Direct action of genistein on CFTR. Pflugers Arch. **434:** 484–491
9 Gribkoff V. K., Champigny G., Barbry P., Dworetzky S. I., Meanwell N. A. and Lazdunski, M. (1994) The substituted benzimidazolone NS004 is an opener of the cystic fibrosis chloride channel. J. Biol. Chem. **269:** 10983–10986
10 Ma T., Vetrivel L., Yang H., Pedemonte N., Zegarra-Moran O., Galietta, L. J. V. et al. (2002) High-affinity activators of cystic fibrosis transmembrane conductance regulator (CFTR) chloride conductance identified by high-throughput screening. J. Biol. Chem. **277:** 37235–37241
11 Galietta L. J., Springsteel M. F., Eda M., Niedzinski E. J., By K., Haddadin M. J. et al. (2001) Novel CFTR chloride channel activators identified by screening of combinatorial libraries based on flavone and benzoquinolizinium lead compounds. J. Biol. Chem. **276:** 19723–19728
12 Cai Z. and Sheppard D. N. (2002) Phloxine B interacts with the cystic fibrosis transmembrane conductance regulator at multiple sites to modulate channel activity. J. Biol. Chem. **277:** 19546–19553
13 Becq F., Mettey Y., Gray, M. A., Galietta L. J., Dormer R. L., Merten M. et al. (1999) Development of substituted benzo[c]quinolizinium compounds as novel activators of the cystic fibrosis chloride channel. J. Biol. Chem. **274:** 27415–27425
14 Lansdell K. A., Cai Z., Kidd J. F. and Sheppard D. N. (2000) Two mechanisms of genistein inhibition of cystic fibrosis transmembrane conductance regulator Cl-channels expressed in murine cell line. J. Physiol. **524:** 317–330
15 Wang F., Zeltwanger S., Yang I. C.-H., Nairn A. C. and Hwang T.-C. (1998) Actions of genistein on cystic fibrosis transmembrane conductance regulator channel gating: evidence for two binding sites with opposite effects. J. Gen. Physiol. **111:** 477–490
16 Ai T., Bompadre S. G., Wang X., Hu S., Li M. and Hwang T. C. (2004) Capsaicin potentiates wild-type and mutant cystic fibrosis transmembrane conductance regulator chloride-channel currents. Mol. Pharmacol. **65:** 1415–1426
17 Tummler B., Dork T., Kubesch P., Fislage R., Kalin N., Neumann T. et al. (1993) Cystic fibrosis: the impact of analytical technology for genotype-phenotype studies. Clin. Chim. Acta **217:** 23–28
18 Zegarra-Moran O., Romio L., Folli C., Caci E., Becq F., Vierfond J. M. et al. (2002) Correction of G551D-CFTR transport defect in epithelial monolayers by genistein but not by CPX or MPB-07. Br. J. Pharmacol. **137:** 504–512
19 Al-Nakkash L., Hu S., Li M. and Hwang T. C. (2001) A common mechanism for cystic fibrosis transmembrane conductance regulator protein activation by genistein and benzimidazolone analogs. J. Pharmacol. Exp. Ther. **296:** 464–47
20 Lewis H. A., Buchanan S. G., Burley S. K., Conners K., Dickey M., Dorwart M. et al. (2004) Structure of nucleotide-binding domain 1 of the cystic fibrosis transmembrane conductance regulator. EMBO J. **23:** 282–293
21 Higgins C. F. (1992) ABC transporters: from microorganisms to man. Annu Rev Cell Biol. **8:** 67–113
22 Loo T. W., Bartlett M. C. and Clarke D. M. (2002) The 'LSGGQ'motif in each nucleotide-binding domain of human P-glycoprotein is adjacent to the opposing walker A sequence. J. Biol. Chem. **277:** 41303–41306
23 Powe A. C. Jr, Al-Nakkash L., Li M. and Hwang T. C. (2002) Mutation of Walker-A lysine 464 in cystic fibrosis transmembrane conductance regulator reveals functional interaction between its nucleotide-binding domains. J Physiol. **539:** 333–346
24 Jones P. M. and George A. M. (1999) Subunit interactions in ABC transporters: towards a functional architecture. FEMS Lett. **179:** 187–202
25 Hopfner K. P., Karcher A., Shin D. S., Craig L., Arthur L. M., Carney J. P. et al. (2000) Structural biology of Rad50 ATPase: ATP-driven conformational control in DNA double-strand break repair and the ABC-ATPase superfamily. Cell **101:** 789–800
26 Smith P. C., Karpowich N., Millen L., Moody J. E., Rosen J., Thomas P. J. et al. (2002) ATP binding to the motor domain from an ABC transporter drives formation of a nucleotide sandwich dimer. Mol. Cell. **10:** 139–149
27 Yuan Y. R., Blecker S., Martsinkevich O., Millen L., Thomas P. J. and Hunt J. F. (2001) The crystal structure of the MJ0796 ATP-binding cassette: implications for the structural consequences of ATP hydrolysis in the active site of an ABC transporter. J. Biol. Chem. **276:** 32313–32321
28 Logan J., Hiestand D., Daram P., Huang Z., Muccio D. D., Hartman J. et al. (1994) Cystic fibrosis transmembrane conductance regulator mutations that disrupt nucleotide binding. J. Clin. Invest. **94:** 228–236
29 Kembi F. and Harrington M. A. (2001) Interdomain but not intermolecular interactions observed in CFTR channels. Biochem. Biophys. Res. Commun. **288:** 819–826
30 Wang W., He Z., O'Shaughnessy T. J., Rux J. and Reenstra W. W. (2002) Domain-domain associations in cystic fibrosis transmembrane conductance regulator. Am. J. Physiol. Cell Physiol. **282:** C1170–C1180
31 Ren X. Q., Furukawa T., Haraguchi M., Sumizawa T., Aoki S., Kobayashi M. et al. (2004) Function of the ABC signature sequences in the human multidrug resistance protein 1. Mol. Pharmacol. **65:** 1536–1542
32 Schmitt L. and Tampe R. (2002) Structure and mechanism of ABC transporters. Curr. Opin. Struct. Biol. **12:** 754–760
33 Sheppard D. N., Rich D. P., Ostedgaard L. S., Gregory R. J., Smith A. E. and Welsh M. J. (1993) Mutations in CFTR associated with mild-disease-form $Cl^-$ channels with altered pore properties. Nature **362:** 160–164
34 Illek B., Lizarzaburu M. E., Lee V., Nantz M. H., Kurth M. J. and Fischer H. (2000) Structural determinants for the activation and block of CFTR-mediated chloride currents by apigenin. Am. J. Physiol. **279:** C1838–C1846

35 Marti-Renom M. A., Stuart A., Fiser A., Sánchez R., Melo F. and Sali A. (2000) Comparative protein structure modeling of genes and genomes. Annu. Rev. Biophys. Biomol. Struct. **29:** 291–325

36 McLachlan A. D. (1982) Rapid comparison of protein structres. Acta Cryst. **A38:** 871–873

37 Guex N. and Peisch M. C. (1997) SWISS-MODEL and the Swiss-PdbViewer: an environment for comparative protein modeling. Electrophoresis **18:** 2717–2723

38 Moran O. (2001) Molecular simulation of the interaction of κ-conotoxin PVIIA to the Shaker potassium channel. Eur. Biophys. J. **30:** 528–536

39 Moran O., Traverso S., Elia L. and Pusch M. (2003) Molecular modeling of p-chlorophenoxyacetic acid binding to the CLC-0 channel. Biochemistry **42:** 5176–5185

40 Kalé L., Skeel R., Bhandarkar M., Brunner R., Attila Gursoy A., Krawetz N. et al. (1999) NAMD2: greater scalability for parallel molecular dynamics. J. Comp. Physiol. **151:** 283–312

41 Wang J., Cieplak P. and Kollman P. A. (2000) How well does restrained electrostatic potential (RESP) model perform in calculating conformational energies of organic and biological compounds? J. Comput. Chem. **21:** 1049–1074

42 Ryckaert J., Bellemans A., Ciccotti G. and Paolini G. V. (1988) Shear-rate dependence of the viscosity of simple fluids by nonequilibrium molecular dynamics. Phys. Rev. Lett. **60:** 128–131

43 Hooft R. W. W., Vriend G., Sander C. and Abola E. E. (1996) Errors in protein structures. Nature. **381:** 272

44 Vriend G. (1990) WHAT IF: a molecular modelling and drug design program. J. Mol. Graph. **8:** 52–56

45 Laskowski R. A., MacArthur M. W., Moss D. S. and Thornton J. M. (1993) PROCHECK: a program to check the stereochemical quality of protein structures. J. Appl. Cryst. **26:** 283–291

46 Casewit C. J., Colwell K. S. and Rappe A. K. (1992) Application of a universal force field to organic molecules. J. Am. Chem. Soc. **114:** 10035–10046

47 Wang J., Wolf R. M., Caldwell J. W., Kollman P. A. and Case D. A. (2004) Development and testing of a general amber force field. J. Comput. Chem. **25:** 1157–1174

48 Katchalski-Katzir E., Shariv, I., Eisenstein M., Friesem A. A., Aflalo C. and Vakser I. A. (1992) Molecular surface recognition: determination of geometric fit between proteins and their ligands by correlation techniques. Proc. Natl. Acad. Sci. USA **89:** 2195–2199

49 Baxter C. A., Murray C. W., Clark D. E., Westhead D. R. and Eldridge M. D. (1998) Flexible docking using Tabu search and an empirical estimate of binding affinity. Proteins **33:** 367–382

50 Eldridge M. D., Murray C. W., Auton T. R., Paolini G. V. and Mee R. P. (1997) Empirical scoring functions. I. The development of a fast empirical scoring function to estimate the binding affinity of ligands in receptor complexes. J. Comput. Aided Mol. Des. **11:** 425–445

51 Jones G., Willett P., Glen R. C., Leach A. R. and Taylor R. (1997) Development and validation of a genetic algorithm for flexible docking. J. Mol. Biol. **267:** 727–748

52 Jones G., Willett P. and Glen R. C. (1995) Molecular recognition of receptor sites using a genetic algorithm with a description of desolvation. J. Mol. Biol. **245:** 43–53

53 Feig M., Onufriev A., Lee M. S., Im W., Case D. A. and Brooks C. L. 3rd (2004) Performance comparison of generalized born and Poisson methods in the calculation of electrostatic solvation energies for protein structures. J. Comput. Chem. **25:** 265–284

54 Onufriev A., Bashford D. and Case D. A. (2004) Exploring protein native states and large-scale conformational changes with a modified generalized born model. Proteins. **55:** 383–394

55 Srinivasan J., Cheatham T. E., Cieplak P., Kollman P. A. and Case D. A. (1998) Continuum solvent studies of the stability of DNA, RNA and phosphoramidate-DNA helices. J. Am. Chem. Soc. **120:** 9401–9409

56 Wang W. and Kollman P. A. (2000) Free energy calculations on dimer stability of the HIV protease using molecular dynamics and a continuum solvent model. J. Mol. Biol. **303:** 567–582

57 Reyes C. M. and Kollman P. A. (2000) Structure and thermodynamics of RNA-protein binding: using molecular dynamics and free energy analyses to calculate the free energies of binding and conformational change. J. Mol. Biol. **297:** 1145–1158

58 Hubbard S. J. and Thornton M. J. (1993) Naccess, a computer program. Department of Biochemistry and Molecular Biology, University College, London

59 Springsteel M. F., Galietta L. J., Ma T., By K., Berger G. O., Yang H. et al. (2003) Benzoflavone activators of the cystic fibrosis transmembrane conductance regulator: towards a pharmacophore model for the nucleotide-binding domain. Bioorg. Med. Chem. **11:** 4113–4120

60 Krieger L., Nabuurs S. B. and Vriend G. (2003) Homology Modeling, in Structural Bioinformatics, pp. 509–523, Bourne P. E. and Weissig H. (eds), Wiley, Hoboken N. J.

61 Jones P. M. and George A. M. (2004) The ABC transporter structure and mechanism: perspectives on recent research. Cell. Mol. Life Sci. **61:** 682–699

62 Obmolova G., Ban C., Hsieh P. and Yang W. (2000) Crystal structures of mismatch repair protein MutS and its complex with a substrate DNA. Nature. **407:** 703–710

63 Lamers M. H., Perrakis A., Enzlin J. H., Winterwerp H. H.,Wind N. de and Sixma T. K. (2000) The crystal structure of DNA mismatch repair protein MutS binding to a G × T mismatch. Nature **407:** 711–717

64 Liu P. Q. and Ames G. F. (1998) In vitro disassembly and reassembly of an ABC transporter, the histidine permease. Proc. Natl. Acad. Sci. USA **95:** 3495–3500

65 Hung L. W., Wang I. X., Nikaido K., Liu P. Q., Ames G. F. and Kim S. H. (1998) Crystal structure of the ATP-binding subunit of an ABC transporter. Nature **396:** 703–707

66 Chang G. and Roth C. B. (2001) Structure of MsbA from *E. coli*: a homolog of the multidrug resistance ATP binding cassette (ABC) transporters. Science **293:** 1793–1800

67 Karpowich N., Martsinkevich O., Millen L., Yuan Y. R., Dai P. L., MacVey K. et al. (2001) Crystal structures of the MJ1267 ATP binding cassette reveal an induced-fit effect at the ATPase active site of an ABC transporter. Structure **9:** 571–586

68 Locher K. P., Lee A. T. and Rees D. C. (2002) The *E. coli* BtuCD structure: a framework for ABC transporter architecture and mechanism. Science **296:** 1091–1098

69 Novotny J., Bruccoleri R. E. and Saul F. A. (1989) On the attribution of binding energy in antigen-antibody complexes McPC 603, D1.3, and HyHEL-5. Biochemistry **28:** 4735–4749

70 Szabo K., Szakacs G., Hegeds T. and Sarkadi B. (1999) Nucleotide occlusion in the human cystic fibrosis transmembrane conductance regulator: different patterns in the two nucleotide binding domains. J. Biol. Chem. **274:** 12209–12212

71 Aleksandrov L., Mengos A., Chang X., Aleksandrov A. and Riordan J. R. (2001) Differential interactions of nucleotides at the two nucleotide binding domains of the cystic fibrosis transmembrane conductance regulator. J. Biol. Chem. **276:** 12918–12923

72 Aleksandrov L., Aleksandrov A. A., Chang X. B. and Riordan J. R. (2002) The first nucleotide binding domain of cystic fibrosis transmembrane conductance regulator is a site of stable nucleotide interaction, whereas the second is a site of rapid turnover. J. Biol. Chem. **277:** 15419–15425

73 Caci E., Folli C., Zegarra-Moran O., Ma T., Springsteel M. F., Sammelson R. E. et al. (2003) CFTR activation in human bronchial epithelial cells by novel benzoflavone and benzimidazolone compounds. Am. J. Physiol. Lung Cell Mol. Physiol. **285:** L180–L188

74 Rossmann M. G., Moras D. and Olsen K. W. (1974) Chemical and biological evolution of nucleotide-binding protein. Nature **250:** 194–199
75 Bianchet M. A., Ko Y. H., Amzel L. M. and Pedersen P. L. (1997) Modeling of nucleotide binding domains of ABC transporter proteins based on a F1-ATPase/recA topology: structural model of the nucleotide binding domains of the cystic fibrosis transmembrane conductance regulator (CFTR). J. Bioenerg. Biomembr. **29:** 503–524
76 Callebaut I., Eudes R., Mornon J. P. and Lehn P. (2004) Nucleotide-binding domains of human cystic fibrosis transmembrane conductance regulator: detailed sequence analysis and three-dimensional modeling of the heterodimer. Cell. Mol. Life Sci. **61:** 230–242
77 Vergani P., Nairn A. C. and Gadsby D. C. (2003) On the Mechanism of MgATP-dependent gating of CFTR $Cl^-$ channels. J. Gen. Physiol. **121:** 17–36
78 Fetsch E. E. and Davidson A. L. (2003) Maltose transport through the inner membrane of *E. coli.* Front. Biosci. **8:** d652–d660
79 Moody J. E., Millen L., Binns D., Hunt J. F. and Thomas P. J. (2002) Cooperative, ATP-dependent association of the nucleotide binding cassettes during the catalytic cycle of ATP-binding cassette transporters. J. Biol. Chem. **277:** 21111–2114
80 Moran O. and Zegarra-Moran O. (2003) Molecular model of the nucelotide binding domains of the CFTR: cystic fibrosis correlated mutations. Pediat Pulmonol. **Suppl. 25:** 197
81 Ferrara P., Gohlke H., Price D. J., Klebe G. and Brooks C. L. 3rd (2004) Assessing scoring functions for protein-ligand interactions. J. Med. Chem. **47:** 3032–3047
82 Kabsch W. and Sander C. (1983) Dictionary of protein secondary structure: pattern recognition of hydrogen-bonded and geometrical features. Biopolymers **22:** 2577–2637


To access this journal online:
http://www.birkhauser.ch